NACA TN 1954

NATIONAL ADVISORY COMMITTEE FOR AERONAUTICS

TECHNICAL NOTE 1954

EXPERIMENTAL AND THEORETICAL DISTRIBUTION OF FLOW PRODUCED BY INLET GUIDE VANES OF AN AXIAL-FLOW COMPRESSOR

By Harold B. Finger, Harold J. Schum, and Howard A. Buckner, Jr.

Lewis Flight Propulsion Laboratory
Cleveland, Ohio

Washington
October 1949

NATIONAL ADVISORY COMMITTEE FOR AERONAUTICS

TECHNICAL NOTE 1954

EXPERIMENTAL AND THEORETICAL DISTRIBUTION OF FLOW PRODUCED BY INLET GUIDE VANES OF AN AXIAL-FLOW COMPRESSOR

By Harold B. Finger, Harold J. Schum
and Howard A. Buckner, Jr.

SUMMARY

A cascade investigation has been conducted to determine the performance of a set of inlet guide vanes designed for use in a multistage axial-flow compressor and to compare the performance with that predicted by a cylindrical-cascade evaluation method. The method determines the velocities at the outlet of the blade row when the flow-angle and total-enthalpy distributions are known and when the simplified-radial-equilibrium relation is satisfied. The measured flow angles are compared with the angles predicted by an empirical rule. Radial survey data were obtained at the inlet and the outlet of the guide vanes for specific weight flows of 27.95, 31.78, 36.12, and 38.86 pounds per second per square foot outlet-annulus area.

The effect of weight flow on the radial distributions of total pressure and flow angle was small. The deviation angle was substantially constant over the central portion of the passage but increased toward the tip. For camber angles above 30°, a critical Mach number at which the lift coefficient decreases with increasing Mach number was obtained at a specific weight flow of 38.86 pounds per second per square foot. When the radial distribution of flow angle was known, the guide-vane outlet velocities over the central portion of the passage could be computed by a cylindrical-cascade evaluation method within an accuracy of 2 percent.

INTRODUCTION

The purpose of inlet guide vanes for axial-flow compressors is to deliver the air efficiently to the first row of rotor blades at the desired angles of attack. Although the design of inlet guide vanes should be a relatively simple task in view of the low angles of incidence, the small amount of turning usually required, and the favorable pressure gradient through the blade row, prediction

of performance has been difficult. On the basis of a two-dimensional cascade investigation, design charts that can be used to design inlet guide vanes having specific NACA airfoil sections are presented in reference 1. If no experimental data are available, the designer must use some empirical rule or a potential-flow theory as a basis for the design of guide vanes and the blades are altered as necessitated by experiment.

An investigation was conducted at the NACA Lewis laboratory to provide experimental data on inlet guide vanes where the flow velocities are relatively high and where three-dimensional effects are appreciable. These data are compared to the results predicted by a cylindrical-cascade evaluation method by which the outlet velocities may be determined when the flow-angle and total-enthalpy distributions are known. The method is applicable to any blade row when simplified radial equilibrium exists. A comparison between the measured flow angles and the angles predicted by a rule that is a revision of Constant's rule (reference 2) and considers the effect of blade stagger on flow angle is also made.

ANALYSIS

The design of an axial-flow-machine blade row requires a knowledge of total-enthalpy, flow-angle, and velocity distributions at the outlet of the preceding blade row. A relation is therefore necessary that can be used to solve for any one of the variables when the others are specified. Because the total enthalpy and the flow angles can be readily measured in an experimental investigation and can be specified in a design procedure, a relation expressing the axial and tangential velocities as functions of enthalpy and flow angle at any given mass flow would facilitate design procedures and the determination of cascade performance.

The following discussion presents the development of such a cylindrical-cascade evaluation method. All symbols are defined in appendix A.

The energy equation for compressible flow can be stated as

$$t = T - \frac{1}{2}\frac{V_\theta^2}{c_p J g} - \frac{1}{2}\frac{V_z^2}{c_p J g} - \frac{1}{2}\frac{V_r^2}{c_p J g} \tag{1}$$

Differentiation of equation (1) with respect to the radius gives

$$\frac{dt}{dr} = \frac{dT}{dr} - \frac{1}{2c_pJg}\frac{d(V_\theta^2)}{dr} - \frac{1}{2c_pJg}\frac{d(V_z^2)}{dr} - \frac{1}{2c_pJg}\frac{d(V_r^2)}{dr} \qquad (2)$$

The fundamental relation between total- and static-gas conditions at a point is given by

$$\frac{P_1^{\frac{\gamma-1}{\gamma}}}{T_1} = \frac{p_1^{\frac{\gamma-1}{\gamma}}}{t_1} = K$$

or

$$\frac{\gamma-1}{\gamma}\log_e P_1 - \log_e T_1 = \frac{\gamma-1}{\gamma}\log_e p_1 - \log_e t_1 = 0$$

Differentiation with respect to the radius and transposition of terms gives

$$\frac{dt_1}{dr} = \frac{\gamma-1}{\gamma}\frac{t_1}{p_1}\frac{dp_1}{dr} = \frac{1}{c_p\,\rho_1}\frac{dp_1}{dr} \qquad (3)$$

Equation (3) requires that the losses be constant along the radius.

If the relation of equation (3) is substituted into equation (2)

$$\left[\frac{dT}{dr} - \frac{1}{2c_pJg}\frac{d(V_\theta^2)}{dr} - \frac{1}{2c_pJg}\frac{d(V_z^2)}{dr} - \frac{1}{2c_pJg}\frac{d(V_r^2)}{dr}\right] = \frac{1}{c_p\,\rho_1}\frac{dp_1}{dr} \qquad (4)$$

For radial equilibrium, if the assumption is made that $\frac{\partial V_r}{\partial r}$ or V_r and $\frac{\partial V_r}{\partial z} = 0$,

$$\frac{1}{\rho}\frac{dp}{dr} = \frac{V_\theta^2}{r} \qquad (5)$$

When $V_r = 0$, equations (4) and (5) combine to yield

$$\frac{dT}{dr} - \frac{1}{2c_pJg}\frac{d(V_\theta^2)}{dr} - \frac{1}{2c_pJg}\frac{d(V_z^2)}{dr} - \frac{1}{c_pJg}\frac{V_\theta^2}{r} = 0 \qquad (6)$$

Equation (6) expresses the relation between the gas velocities and the gas state where radial velocities are negligible and when the losses are constant along the radius.

From the vector-diagram geometry

$$V_\theta = V_z \tan \alpha$$

and

$$\frac{d(V_\theta^2)}{dr} = 2V_z^2 \sec^2 \alpha \tan \alpha \frac{d\alpha}{dr} + \tan^2 \alpha \frac{d(V_z^2)}{dr}$$

Substitution of the geometrical relations into equation (6) gives

$$c_pJg\frac{dT_1}{dr} = \frac{V_z^2}{r}\left(\tan^2 \alpha + r \tan \alpha \sec^2 \alpha \frac{d\alpha}{dr}\right) + \frac{1}{2}\frac{d(V_z^2)}{dr}\sec^2 \alpha$$

Division of the preceding equation by $\frac{1}{2}\sec^2 \alpha$ gives

$$c_pJg\frac{dT_1}{dr}\frac{1}{\sec^2 \alpha} = 2V_z^2\left(\frac{\sin^2 \alpha}{r} + \tan \alpha \frac{d\alpha}{dr}\right) + \frac{d(V_z^2)}{dr} \qquad (7)$$

Let

$$2\left(\frac{\sin^2 \alpha}{r} + \tan \alpha \frac{d\alpha}{dr}\right) = S$$

and

$$\frac{2}{\rho_o}\frac{dP}{dr}\frac{1}{\sec^2 \alpha} = Q$$

Therefore, at any radius, equation (7) will be

$$SV_z^2 + \frac{d(V_z^2)}{dr} = Q$$

or

$$SV_z^2 dr + d(V_z^2) = Q dr$$

which is a first-order differential equation linear in V_z^2 that has the following solution:

$$\left[V_z^2 \exp\left(\int_{r_h}^{r} S \, dr \right) \right]_{r_h}^{r} = \int_{r_h}^{r} Q \exp\left(\int_{r_h}^{r} S \, dr \right) dr$$

If the values of S and Q are substituted

$$\left\{ V_z^2 \exp\left[\int_{r_h}^{r} \left(\frac{2 \sin^2 \alpha}{r} + 2 \tan \alpha \frac{d\alpha}{dr} \right) dr \right] \right\}_{r_h}^{r}$$

$$= \int_{T_h}^{T} \frac{2 c_p J g \, dT}{\sec^2 \alpha} \exp\left[\int_{r_h}^{r} \left(\frac{2 \sin^2 \alpha}{r} + 2 \tan \alpha \frac{d\alpha}{dr} \right) dr \right] \tag{8}$$

The exponential in equation (8) can be integrated as follows:

$$\int_{r_h}^{r} \left(\frac{2 \sin^2 \alpha}{r} + 2 \tan \alpha \frac{d\alpha}{dr} \right) dr = \int_{r_h}^{r} 2 \sin^2 \alpha \frac{dr}{r} - \left[2 \log_e \cos \alpha \right]_{\alpha_h}^{\alpha}$$

$$= \int_{r_h}^{r} 2 \sin^2 \alpha \frac{dr}{r} + 2 \log_e \left(\frac{\cos \alpha_h}{\cos \alpha} \right)$$

Therefore

$$\exp\left[\int\left(\frac{2\sin^2\alpha}{r}+2\tan\alpha\frac{d\alpha}{dr}\right)dr\right]=\left(\frac{\cos\alpha_h}{\cos\alpha}\right)^2\exp\left(\int_{r_h}^{r}2\sin^2\alpha\frac{dr}{r}\right) \tag{9}$$

By application of equation (9), equation (8) reduces to

$$\left[V_z{}^2\left(\frac{\cos\alpha_h}{\cos\alpha}\right)^2\exp\left(\int_{r_h}^{r}2\sin^2\alpha\frac{dr}{r}\right)\right]_{r_h}^{r}$$

$$=\int_{T_h}^{T}2c_pJg\cos^2\alpha_h\exp\left(\int_{r_h}^{r}2\sin^2\alpha\frac{dr}{r}\right)dT$$

This equation can be further reduced to

$$V_z{}^2\left(\frac{\cos\alpha_h}{\cos\alpha}\right)^2\exp\left(\int_{r_h}^{r}2\sin^2\alpha\frac{dr}{r}\right)-V_{z,h}{}^2$$

$$=\int_{T_h}^{T}2c_pJg\cos^2\alpha_h\exp\left(\int_{r_h}^{r}2\sin^2\alpha\frac{dr}{r}\right)dT \tag{10}$$

From the continuity equation

$$W=\int_{r_h}^{r_t}2\pi r\,dr\,\rho gV_z=\int_{r_h^2}^{r_t^2}\pi\rho gV_z\,d(r^2) \tag{11}$$

As a first approximation, ρ will be assumed constant along the radius and equal to a value indicated by a wall static-pressure measurement in order to reduce the number of trials necessary.

Equations (10) and (11) can be simultaneously solved by a trial-and-error method. An assumed value of $V_{z,h}$ is substituted in equation (10) so that V_z can be determined as a function of the radius. The term $\int_{r_h^2}^{r_t^2} \pi\rho g V_z \, d(r^2)$ can then be calculated and its value checked by the continuity relation given in equation (11). This procedure is repeated until the values of the integrals determined by the two methods check.

A new radial distribution of density can be determined by combining the energy equation and isentropic relation to give

$$\frac{\rho}{\rho_o} = \left[1 - \frac{(\gamma-1)}{2} \frac{V^2}{\gamma g R T}\right]^{\frac{1}{\gamma-1}}$$

or

$$\frac{\rho}{\rho_o} = \left[1 - \frac{(\gamma-1)}{2} \frac{V_z^2}{\gamma g R T \cos^2 \alpha}\right]^{\frac{1}{\gamma-1}} \tag{12}$$

The distribution of density determined from equation (12) is then substituted in equation (11) and the procedure is repeated until the final density distribution checks the one used in the continuity equation. The velocity distribution can be determined from the known distributions of total enthalpy and outlet angle.

The preceding solution can be used to determine the flow from any blade row, rotor, or stator (if the simplified-radial-equilibrium relation is satisfied). In a design procedure, the conditions upstream of the rotor are usually prescribed. Then, by specifying the distribution of work in the rotor the distribution of total enthalpy downstream of the rotor is determined. The radial distribution of absolute flow angle is generally specified by the type of flow desired so that the method of determining the velocity distributions can be used as part of a design procedure. Corrections could be made for boundary layers at the annulus walls by assuming the distribution of total enthalpy in the boundary layer and substituting in equation (10), or more simply by applying a correction factor in the continuity relation.

If the total temperature is practically constant along the radius, as was the case in the present investigation, equation (10) becomes

$$V_z^2 \frac{\cos \alpha_h}{\cos \alpha} \exp\left(\int_{r_h}^{r} 2 \sin^2 \alpha \frac{dr}{r}\right) - V_{z,h}^2 = 0$$

and

$$\frac{V_z}{V_{z,h}} = \frac{\cos \alpha}{\cos \alpha_h} \exp\left(\int_{r}^{r_h} \sin^2 \alpha \frac{dr}{r}\right) \tag{13}$$

The axial velocity at the hub can be determined from the continuity relation

$$V_{z,h} = \frac{W}{2\pi g \int_{r_h}^{r_t} \rho \frac{V_z}{V_{z,h}} r \, dr} \tag{14}$$

The density distribution is determined by the trial-and-error method previously discussed in the general solution of the equations. In this investigation, it was found that the radial variation of density could be neglected.

Because the flow angle from the guide vanes is practically constant over a large range of inlet Mach numbers or weight flows, the exponential in equation (13) and the resulting ratio of axial velocities need be evaluated only once.

The radial distribution of axial velocity was determined in the present investigation by combining equations (13) and (14) and solving graphically.

APPARATUS AND PROCEDURE

Inlet guide vanes. - The inlet guide vanes used in the investigation were designed for an axial-flow compressor with a specific weight flow at the first row of rotor blades of approximately 40 pounds of air per second per square foot of annulus area at

sea-level inlet-air conditions. The blades of the guide-vane cascade are shrouded at both the tip and the root. These shrouds are tapered to form an annular flow area that converges between the inlet and the outlet of the cascade. The outlet tip-to-hub radius ratio of the guide vanes is 2.0. The solidity of the guide vanes varies from 1.75 at a radius ratio of 1.0 to 1.0 at a radius ratio of 1.8.

The airfoil sections have a parabolic-arc camber line. The trailing edges of the blades are on a radial line. The blade-camber angle varies from approximately 25° at the root to 35° at the tip and the stagger angle (angle between chord and axial direction) varies from approximately 12° to 20°. The maximum thickness is of the order of 6 percent of the chord length and occurs at approximately 35 percent of the chord. The maximum camber occurs at approximately 40 percent of the chord.

Setup. - A diagrammatic drawing of the setup used in the investigation of the flow through the guide vanes is shown in figure 1. The guide-vane cascade was mounted in a cast-aluminum inlet section (fig. 1). A hemispherical hub was attached to the entrance of the inlet section. The straight annular air passage in the inlet section faired smoothly into the guide-vane cascade. The inlet section had four airfoil-shaped struts that would normally support the compressor front-bearing housing and accessory drive.

Ambient air entered the unit through a thin-plate orifice mounted on the intake end of an orifice tank, 3 feet in diameter and 12 feet in length. A $13\frac{1}{2}^{\circ}$ conical reducer, $17\frac{1}{2}$ inches in length, was fitted between the orifice tank and the inlet section to provide a favorable pressure gradient in the direction of flow. The inlet section with the guide vanes in position was bolted to a discharge adapting section made annular by a wood inner cylinder. The inner and outer diameters of this annular discharge passage simulated those of the hub and the casing of the first stage in the axial-flow compressor. The length of the annular discharge passage was $14\frac{1}{2}$ inches. The air was discharged through an elbow into the laboratory altitude exhaust system. A 1/2-inch-mesh 75-percent opening screen was located immediately upstream of the elbow to reduce circumferential variations.

Instrumentation. - The setup was instrumented to determine the following quantities: gas state upstream of the flow-measuring orifice, static-pressure drop across the orifice, gas state at the inlet measuring station upstream of the blade row, radial variation in velocity at the inlet measuring station, circumferential distribution of static pressure on the inner

and outer walls at inlet and outlet measuring stations, gas state at outlet measuring station, and the radial variations of velocity and flow angle at the outlet measuring station.

The inlet-air temperature was measured with a liquid-in-glass thermometer. A wall static tap located according to reference 4 was used to measure the orifice pressure drop, which was indicated on a water manometer.

The inlet measuring station was located in the straight annular portion of the compressor-inlet section, approximately $1\frac{1}{2}$ chord lengths upstream of the leading edge of the guide vanes, as shown in figure 1. Four wall static-pressure taps were located at this station between struts on both the inner and outer walls, $22\frac{1}{2}^{\circ}$ apart; the taps on the outer wall were located on the same radial elements as those of the inner wall. A hook-type static-pressure probe (fig. 2(a)) and a shielded total-pressure probe (fig. 2(b)) insensitive to yaw to approximately $\pm 45^{\circ}$ were located at this station to measure the radial pressure distribution.

The outlet measuring station was located in a plane approximately 2 chord lengths downstream of the trailing edge of the guide vanes (fig. 1). Four wall static-pressure taps were located at this station on both the inner and outer walls and in the same axial planes as those of the inlet station. A static-pressure probe of the type used at the inlet was also located at this station. In addition, a two-hole Fechheimer tube (fig. 2(c)) was used to measure the radial distribution of flow angle and total pressure.

Instrumentation was located to avoid measurement in the wakes of the airfoil sections. Inlet pressures were indicated on a common-well water manometer board; outlet pressures were indicated on mercury manometers.

Procedure. - Survey runs were made at values of specific weight flow of 27.95, 31.78, 36.12, and 38.86 pounds per second per square foot annulus area, which are in the high weight-flow range for these guide vanes. Air flow was regulated by a butterfly throttle valve in the exhaust line. The weight flow was maintained constant to within ± 0.5 percent while the various measurements were made. The Reynolds numbers, based on the outlet conditions encountered in the present investigation with the blade chord as the characteristic dimension, were in the range of 300,000 to 500,000. The effects of variation of Reynolds number in this range were assumed to be small.

Precision. - The accuracy with which all measurements were made is estimated to be within the following limits:

Inlet pressure, inches of water	±0.05
Outlet pressure, inches of mercury	±0.05
Flow angle, degrees	±1.0
Weight flow, percent	±0.5
Velocity, percent	±0.5

Calibration of the static-pressure probe showed that the maximum error of the instrument up to an indicated Mach number of about 0.75 was 2 percent of the indicated velocity pressure. The shielded total-pressure probe used at the inlet station was found to be insensitive to yaw to approximately ±45°.

A further error was induced by assuming that radial surveys at corresponding points between adjacent blades were sufficient for specifying the cascade performance. Because no circumferential surveys were made, the data could not be corrected for circumferential variations. An indication of the effect of circumferential position was obtained from measurements of wall static pressure that gave variations around the inner and outer walls of as much as 12 percent of the velocity pressure, which resulted in a maximum variation in velocity of approximately ±2 percent. These random circumferential variations were caused by inaccuracies in setting the vanes in position. Measurements indicated that the blade-angle settings varied as much as 3° or $3\frac{1}{2}$°. It is believed that the blade spacing also varied appreciably. Additional variations may have been introduced by the elbow behind the test section.

Calculations. - The weight of air flowing through the guide vanes was computed from the orifice data by the method recommended in reference 3. This weight-flow determination was checked by integrating the velocity profiles at the inlet and the outlet of the guide vanes. In general, the inlet-station measurements checked the orifice measurement within 2 percent and the corresponding agreement with the measurements at the outlet station was within 3 percent.

Values of absolute velocity were calculated from the static- and total-pressure measurements by using the relation

$$V = \sqrt{\frac{2\gamma gRT}{\gamma-1}\left[1-\left(\frac{p}{P}\right)^{\frac{\gamma-1}{\gamma}}\right]}$$

based on the Bernoulli equation and the isentropic gas laws. Axial and tangential velocities were computed from the resultant velocity and the measured flow angle.

The following expression, which is derived in appendix B, was used to determine lift coefficients for the guide vanes:

$$C_L = \frac{8 \frac{s}{c} \frac{V_2}{V_i} \sin \alpha_2}{\left(1 + \frac{V_2}{V_i} \cos \alpha_2\right)\sqrt{\left(1 + \frac{V_2}{V_i} \cos \alpha_2\right)^2 + \left(\frac{V_2}{V_i} \sin \alpha_2\right)^2}}$$

This equation assumed that the lift force is perpendicular to the vectorial mean of the inlet and outlet velocities. This assumed lift differs slightly from the theoretical force resulting from momentum and pressure considerations.

RESULTS AND DISCUSSION

Guide-Vane Performance

The results of the investigation are presented as radial distributions of pressures, angles, velocities, and lift coefficients.

Inlet survey data. - The results of the surveys at the inlet measuring station for the specific weight flows investigated are presented in figures 3 to 5. Curves of inlet total and inlet static pressure divided by atmospheric pressure are shown in figures 3 and 4, respectively, as functions of the ratio of the radius at any point in the flow passage to the hub radius. Figure 5 presents the velocity of the air at the inlet measuring station plotted against the radius ratio.

The inlet total pressure was fairly constant over most of the flow passage, decreasing slightly as the air weight flow was increased. At the tip, however, there was a marked decrease in total pressure, probably resulting from viscous effects at the duct wall upstream of the measuring station. In any case, the nonuniform inlet-total-pressure distribution did not appreciably affect the results at the outlet because calculations have indicated that the maximum change in resultant outlet velocity due to the nonuniform profile was less than 5 percent.

The radial distribution of inlet static pressure (fig. 4) is of the form that might be expected from flow upstream of a convergent channel; that is, the static pressure at the center of the passage is less than that at either wall.

The radial distribution of velocity at the inlet measuring station is presented in figure 5 for the four weight flows investigated. The inlet velocities were found to have no tangential components. The decrease in inlet velocity near the outer wall follows the same form as that of the inlet-total pressure distribution. The velocities immediately upstream of the guide vanes can be computed from the data taken at the inlet measuring station by application of the continuity equation, if incompressible flow and zero incidence are assumed.

Outlet survey data. - The results of the radial surveys at the outlet measuring station are presented in figures 6 to 9 as the ratios of outlet total and static pressure to atmospheric pressure, outlet deviation angle, and outlet velocity plotted against radius ratio. The ratio of outlet total pressure to atmospheric pressure (fig. 6) was approximately constant over the central portion of the annular passage area but dropped in the boundary layer near the tip. A similar situation probably occurred at the inner wall; no data were taken close to the hub, however, because of the configuration of the yaw tube. The total pressure decreased slightly as the weight flow was increased, indicating increased losses.

The static pressure at the outlet measuring station increased uniformly from the hub to the tip of the blades (fig. 7). The slope of the static-pressure variation increased slightly as the flow was increased from 27.95 to 38.86 pounds per second per square foot. As shown in figure 7, the static-pressure gradient at the measuring station (2 chord lengths downstream of the cascade) was practically that gradient which is required for the simplified-radial-equilibrium condition where the radial velocity and the axial variation of radial velocity is negligible. Immediately downstream of the guide vanes, the distribution of static pressure would differ from that at the measuring station because of the radial flow induced by the convergent inner and outer shrouds. For axially symmetric flow, the condition of radial equilibrium of forces immediately behind the guide vane is

$$\frac{1}{\rho}\frac{dp}{dr} = \frac{V_\theta^2}{r} - V_z\frac{\partial Vr}{\partial z} - Vr\frac{\partial Vr}{\partial r}$$

The simplified-radial-equilibrium relation, which was found to exist at the outlet measuring station, assumed that the last two terms in the preceding equation are negligible.

The radial distribution of air-outlet deviation angle (angle between trailing-edge camber line and outlet-air velocity) is presented in figure 8 for the four weight flows investigated. The deviation angle decreased slightly from a radius ratio of 1.1 to a radius ratio of approximately 1.45. At this point, the deviation angle increased slightly until the boundary layer was reached through which the deviation decreased sharply because of the decrease in axial velocity. If the precision of measurement is considered, however, the deviation is practically constant at 2° over the central portion of the passage. For these vanes, the effect of the increasing camber angle from hub to tip is inversely proportional to the effect of the decreasing solidity so that the two factors counterbalance each other and cause the deviation to remain substantially constant. No flow-angle measurements were taken close to the hub because of the Fechheimer instrument geometry, which was such as to prevent tube-end effects on the measurements. The effect of weight flow on the angle distribution was practically negligible giving a maximum over-all variation of 2°. Immediately behind the guide vanes, the effects of the finite blade and wake thicknesses and the boundary layer may give a different flow-angle distribution than that existing at the outlet measuring station.

The radial variations in resultant, axial, and tangential velocities at the outlet measuring station are presented in figure 9 for the air weight flows considered.

The trends of the corresponding velocity distributions are the same for all the flow conditions; the axial and resultant velocities decrease and the tangential component increases with radius ratio. These trends are caused by the effects of solidity on axial velocity and of camber angle on tangential velocity.

Lift coefficient. - The distribution of lift coefficient as computed from the equation developed in appendix B is presented in figure 10 for the four air weight flows investigated as a function of camber angle and solidity. For camber angles below 30° and solidities above 1.2, the effect of weight flow or Mach number on lift coefficient is practically negligible. At higher camber angles, however, the lift coefficient for a specific weight flow of 38.86 pounds per second per square foot is slightly lower than those for specific weight flows of 36.12, 31.78, and 27.95 pounds per second per square foot. The low lift coefficient

at the highest specific weight flow seems to be caused by the attainment of a critical Mach number at which the lift decreases with increase in Mach number. The small effects of Mach number on velocity ratio (resulting from total-pressure loss) and turning angle apparently combine to cause a noticeable effect on lift coefficient.

Comparison of Experimental Results with Analytical Results

The problem of designing accelerating inlet guide vanes is principally one of designing blades that will give a desired flow distribution into the first row of rotor blades. No simple satisfactory method has been devised for the design of guide vanes having any general profile. Experimental investigations such as that of reference 1 have resulted in design procedures that are applicable to the specific airfoils investigated.

Turning angle. - One of the difficulties in inlet-guide-vane design is that of setting the blades to give desired outlet flow angles. The method of redesigning after testing is costly and time-consuming. Empirical design rules based on various theoretical and experimental investigations are most satisfactory because of the ease with which they can be applied. A rule, which is based on potential-flow considerations and is a more exact form of Constant's rule (reference 2), is therefore used herein to determine the deviation angles. Because the blade profile used in this investigation was very similar to the parabolic-arc-cambered airfoil investigated in reference 2, the rule was assumed applicable without further revision by the potential-flow methods. The constant in the rule is a function of the blade stagger angle, which is defined as the angle between the chord and the axial direction. Comparison of the deviation angles predicted by the empirical rule with the measured angles is presented in figure 11 for a specific weight flow of 36.12 pounds per second per square foot. Near the hub, the measured and computed results agree within the precision of measurement. The maximum difference between the measured and computed angles is approximately 3° at a radius ratio of 1.65. The difference then decreases toward the tip and increases in the boundary layer. It must be noted that the derivation of the empirical rule depends on the camber and the stagger of the airfoils in cascade and must be altered by potential-flow methods for each cascade if it is to be made generally applicable.

Velocity. - Outlet velocities can be predicted over the central portion of flow from the cylindrical-cascade evaluation method based on the energy and continuity relations. The application of this equation assumes that the simplified-radial-equilibrium relation is satisfied and that the radial distribution of flow angle is known.

A comparison of the measured and computed axial velocities is presented in figure 12 for a specific weight flow of 36.12 pounds per second per square foot. The analysis was applied to the measured-angle distribution. Over the central portion of the passage, the predicted axial velocities are a maximum of 2 percent lower than the actual velocities but near the outer wall where the total pressure decreases rapidly the agreement is poor. A similar situation probably exists at the inner wall. The error incurred near the midsection is caused by neglecting the boundary-layer effects, which tend to reduce the effective flow area and thereby give higher actual velocities than predicted ones. The problem of designing accelerating guide vanes with constant total pressure and negligible radial flows therefore reduces to that of predicting turning angles. For such guide vanes, the velocities can be accurately determined if the angles are known. The radial velocities must be considered in the radial-equilibrium expression previously discussed if it is applied to a station immediately downstream of the cascade.

SUMMARY OF RESULTS

The results of this investigation of the performance of the inlet guide vanes from a multistage axial-flow compressor can be summarized as follows:

1. The effect of weight flow on the radial distributions of total pressure and flow angle was small. Deviation angle was practically constant over the central portion of the passage but increased near the tip and then decreased rapidly in the boundary layer at the blade tip. The slope of the variation of static pressure with radius increased with increasing weight flow.

2. For camber angles above 30°, a critical Mach number at which the lift coefficient decreases with increasing Mach number was attained at a specific weight flow of 38.86 pounds per second per square foot.

3. If the radial distribution of flow angle is known and if the total pressure is constant, the guide-vane outlet velocities over the central portion of the passage can be computed from the cylindrical-cascade evaluation method within an accuracy of 2 percent.

4. The deviation angles predicted by an empirical rule based on Constant's work were approximately 3° higher than the measured angles. The constant in the rule should be altered by potential-flow methods to make the results applicable for any specific blade profile having a parabolic camber line.

Lewis Flight Propulsion Laboratory,
National Advisory Committee for Aeronautics,
Cleveland, Ohio, July 14, 1948.

APPENDIX A

SYMBOLS

The following symbols were used in the calculations:

A	annulus area, sq ft
C_L	lift coefficient
c	blade chord, ft
c_p	specific heat at constant pressure, Btu/(lb)(^oR)
c_v	specific heat at constant volume, Btu/(lb)(^oR)
D	blade profile drag, lb/ft, (fig. 13)
exp	base of Napierian logarithmic system raised to power in parentheses following exp
F	resultant force on blade element, lb/ft, (fig. 13)
g	acceleration due to gravity, 32.174 ft/sec^2
J	mechanical equivalent of heat, 778 ft-lb/Btu
L	blade profile lift, lb/ft, (fig. 13)
P	total pressure, lb/sq ft absolute
p	static pressure, lb/sq ft absolute
R	gas constant, 53.5 ft-lb/(lb)(^oR)
r	radius, ft
s	blade spacing, ft
T	total temperature, ^oR
t	static temperature, ^oR
V	air velocity, ft/sec, (fig. 13)
W	weight flow, lb/sec

$\frac{W\sqrt{\theta}}{\delta A_2}$ specific weight flow, lb/(sec)(sq ft)

z axial distance

α angle between axial direction and air velocity, deg, (fig. 13)

β blade camber angle, (angle between axial direction and tangent to trailing-edge camber line), deg, (fig. 13)

γ ratio of specific heats, c_p/c_v

Δ deviation angle, $\beta - \alpha_2$, deg, (fig. 13)

δ ratio of atmospheric pressure to standard sea-level pressure, 29.92 in. Hg absolute

θ ratio of atmospheric temperature to standard sea-level temperature, 518.4° R

ρ static density, slugs/cu ft

ρ_o total density, slugs/cu ft

σ solidity, c/s

Subscripts:

0 atmospheric conditions

1 inlet measuring station

2 outlet measuring station

h hub

i immediately upstream of guide vanes

m mean

r radial

t tip

z axial

θ tangential

APPENDIX B

DERIVATION OF LIFT COEFFICIENT

For the purpose of this investigation an expression for lift coefficient as a function of turning angle, solidity, and inlet and outlet velocities was desirable. The derivation of this expression is given in the following paragraphs.

By reference to figure 13, the lift force on the blade is

$$L = \frac{F_\theta}{\cos \alpha_m} + D \tan \alpha_m$$

For low-camber blades with fairly small losses, $D \tan \alpha_m$ is sufficiently small to be neglected with little error. Consequently,

$$L = \frac{F_\theta}{\cos \alpha_m} \tag{B1}$$

The component of the resultant force in the direction perpendicular to axial is given by

$$F_\theta = W (V_{\theta,2} - V_{\theta,i}) \tag{B2}$$

When two-dimensional incompressible flow is assumed, the weight flow per passage and per unit blade length is

$$W = \rho_i g V_i s \tag{B3}$$

Because the flow at the inlet is considered to be axial $V_{\theta,i} = 0$ and $V_{\theta,2} = V_2 \sin \alpha_2$, equations (B2) and (B3) may be combined to obtain

$$F_\theta = \rho_i g V_i^2 s \frac{V_2}{V_i} \sin \alpha_2$$

By substitution in equation (B1),

$$L = \frac{\rho_i g V_i^2 s \frac{V_2}{V_i} \sin \alpha_2}{\cos \alpha_m}$$

Then

$$C_L = \frac{L}{\frac{1}{2}\rho_i g V_m^2 c} = \frac{\rho_i V_i^2 s \frac{V_2}{V_i} \sin \alpha_2}{\frac{1}{2}\rho_i V_m^2 c \cos \alpha_m}$$

From the diagram,

$$V_m = \frac{V_i + V_2 \cos \alpha_2}{2 \cos \alpha_m} = \frac{V_i}{2 \cos \alpha_m}\left(1 + \frac{V_2}{V_i} \cos \alpha_2\right)$$

Therefore

$$C_L = \frac{8\frac{s}{c}\frac{V_2}{V_i} \sin \alpha_2 \cos \alpha_m}{\left(1 + \frac{V_2}{V_i} \cos \alpha_2\right)^2} \tag{B4}$$

Also, from the diagram

$$\cos \alpha_m = \frac{V_i + V_2 \cos \alpha_2}{2\sqrt{\frac{(V_i + V_2 \cos \alpha_2)^2}{4} + \frac{(V_2 \sin \alpha_2)^2}{4}}}$$

$$= \frac{1 + \left(\frac{V_2}{V_i}\right) \cos \alpha_2}{\sqrt{\left(\frac{V_2}{V_i}\right)^2 + 2\left(\frac{V_2}{V_i}\right) \cos \alpha_2 + 1}}$$

By substitution in equation (B4),

$$C_L = \frac{8\frac{s}{c}\frac{V_2}{V_i} \sin \alpha_2}{\left(1 + \frac{V_2}{V_i} \cos \alpha_2\right)\sqrt{\left(1 + \frac{V_2}{V_i} \cos \alpha_2\right)^2 + \left(\frac{V_2}{V_i} \sin \alpha_2\right)^2}}$$

REFERENCES

1. Zimney, Charles M., and Lappi, Viola M.: Data for Design of Entrance Vanes from Two-Dimensional Tests of Airfoils in Cascade. NACA ACR L5G18, 1945.

2. Constant, H.: Note on Performance of Cascades of Aerofoils. Rep. No. E. 3696, R.A.E., June 1939.

3. Ebaugh, N. C., and Whitfield, R.: The Intake Orifice and a Proposed Method for Testing Exhaust Fans. A.S.M.E. Trans., PTC-56-3, vol. 56, no. 12, Dec. 1934, pp. 903-911.

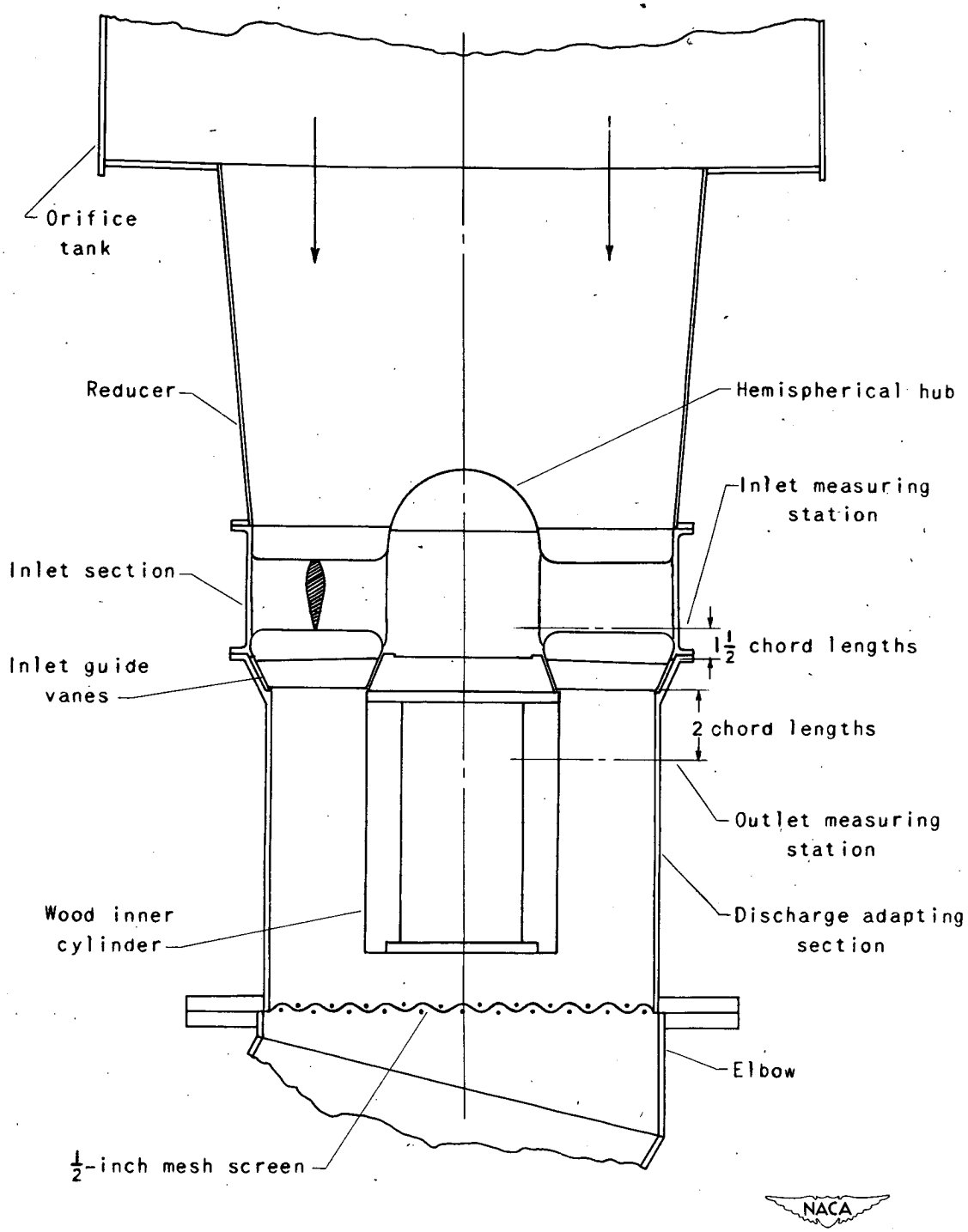

Figure 1. - Schematic drawing of setup.

Page intentionally left blank

Page intentionally left blank

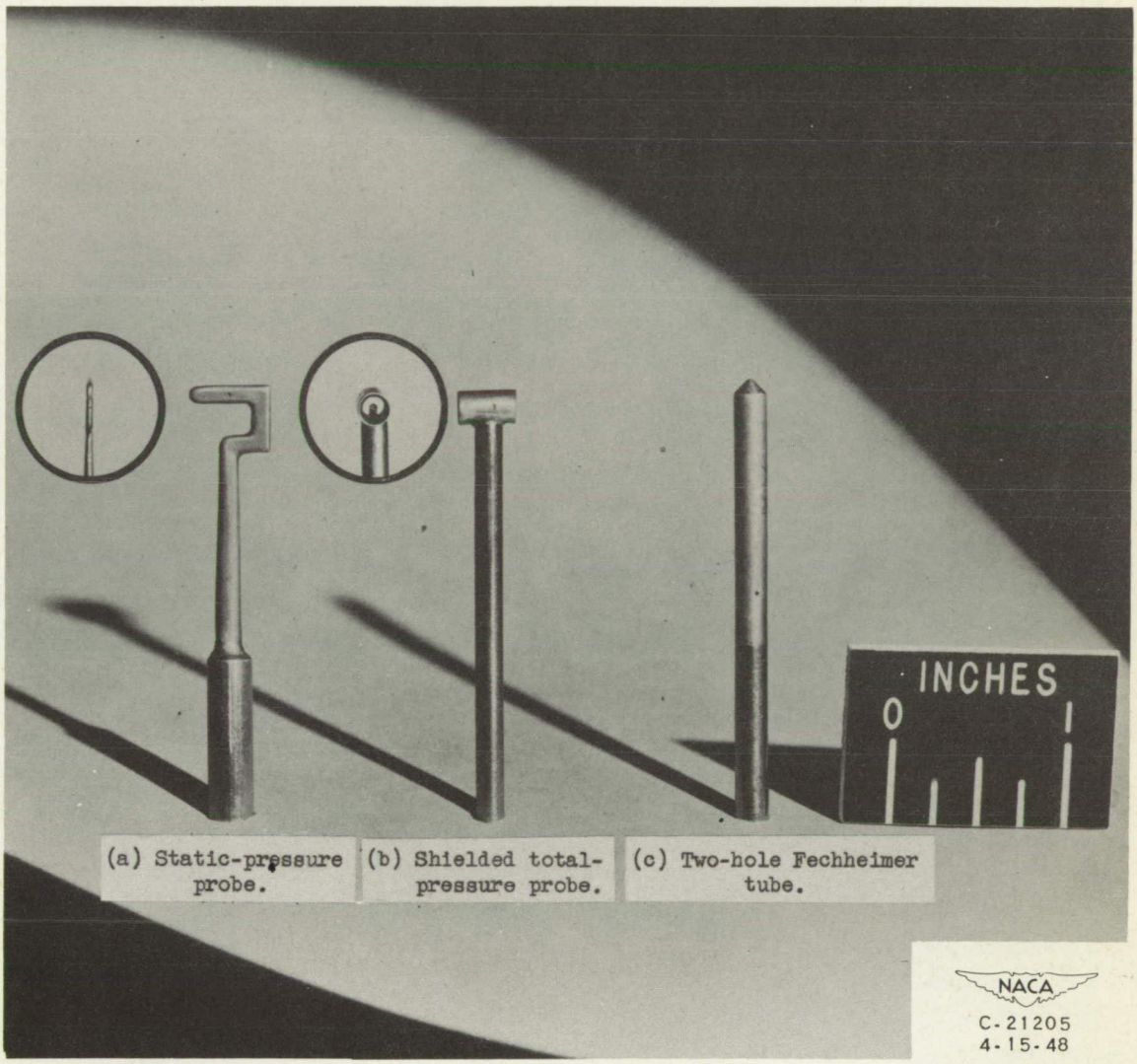

Figure 2. - Radial-survey instruments.

Page intentionally left blank

Page intentionally left blank

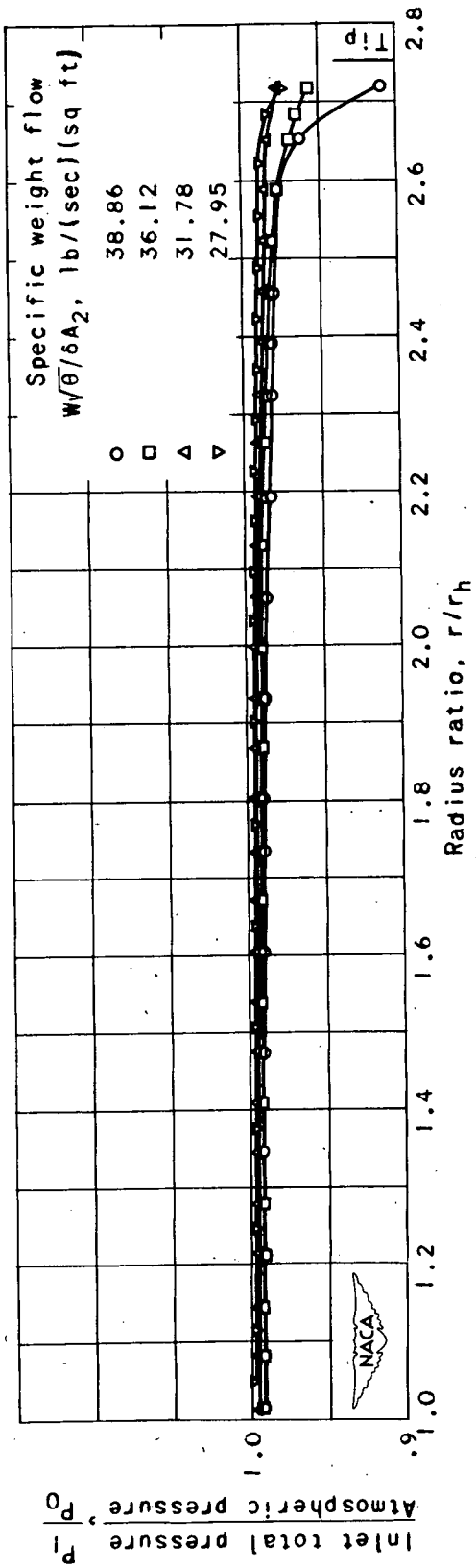

Figure 3. - Radial distribution of ratio of inlet total pressure to atmospheric pressure.

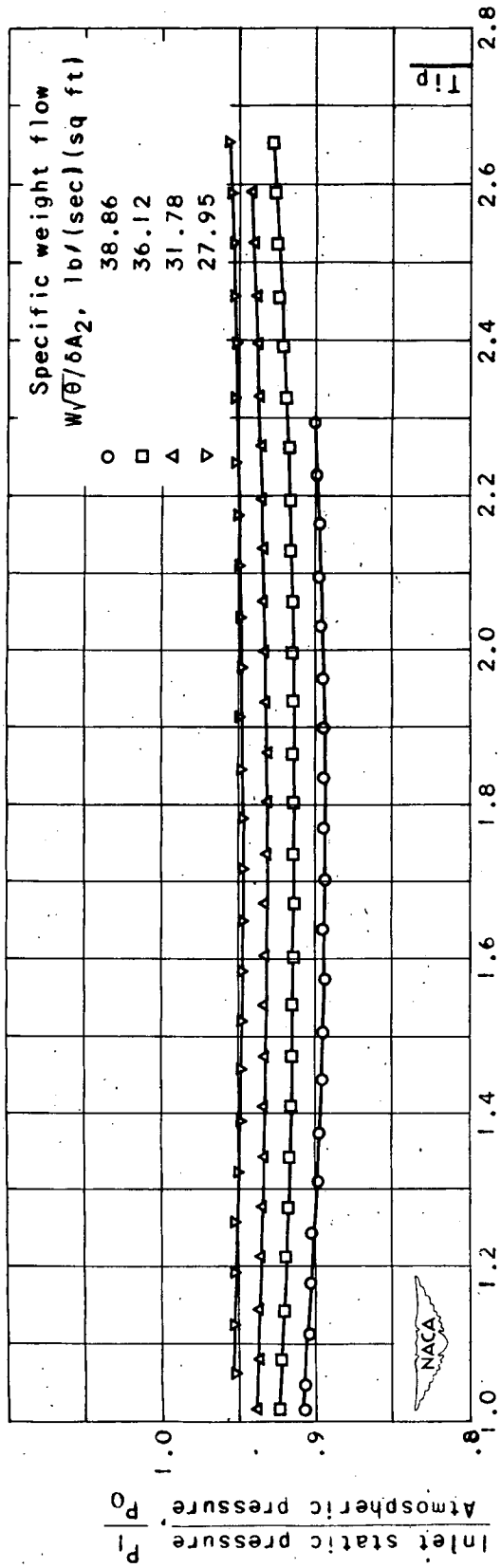

Figure 4. - Radial distribution of ratio of inlet static pressure to atmospheric pressure.

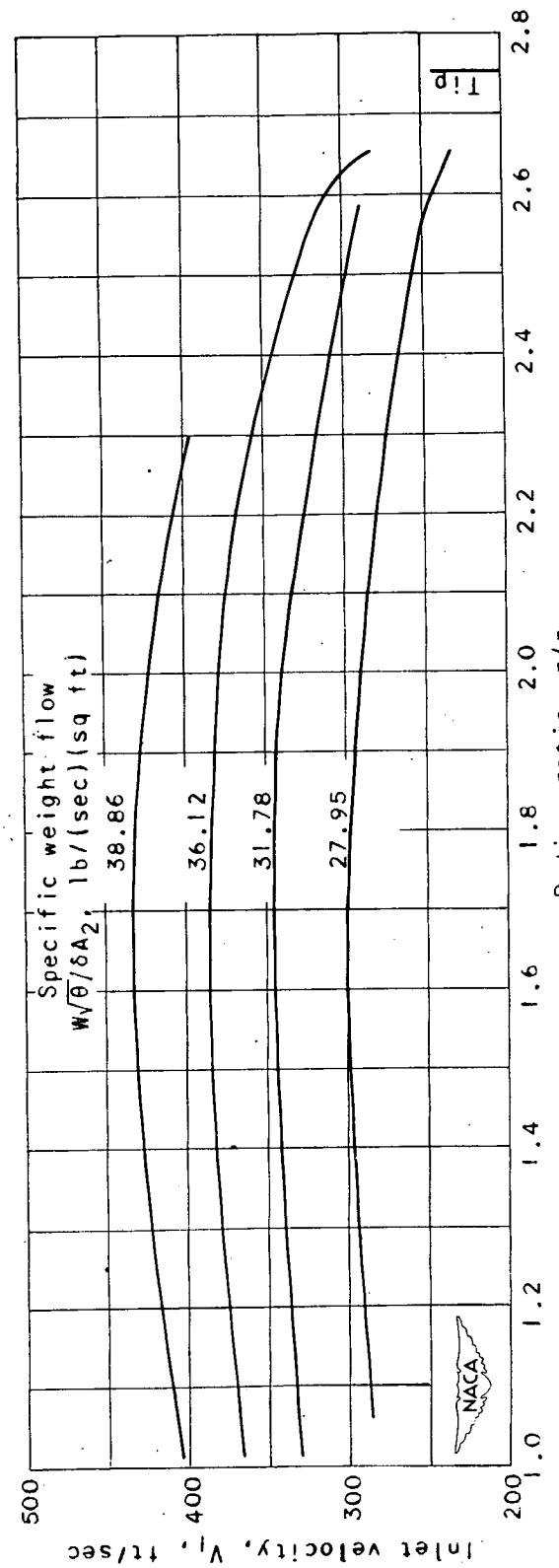

Figure 5. - Radial distribution of inlet velocity.

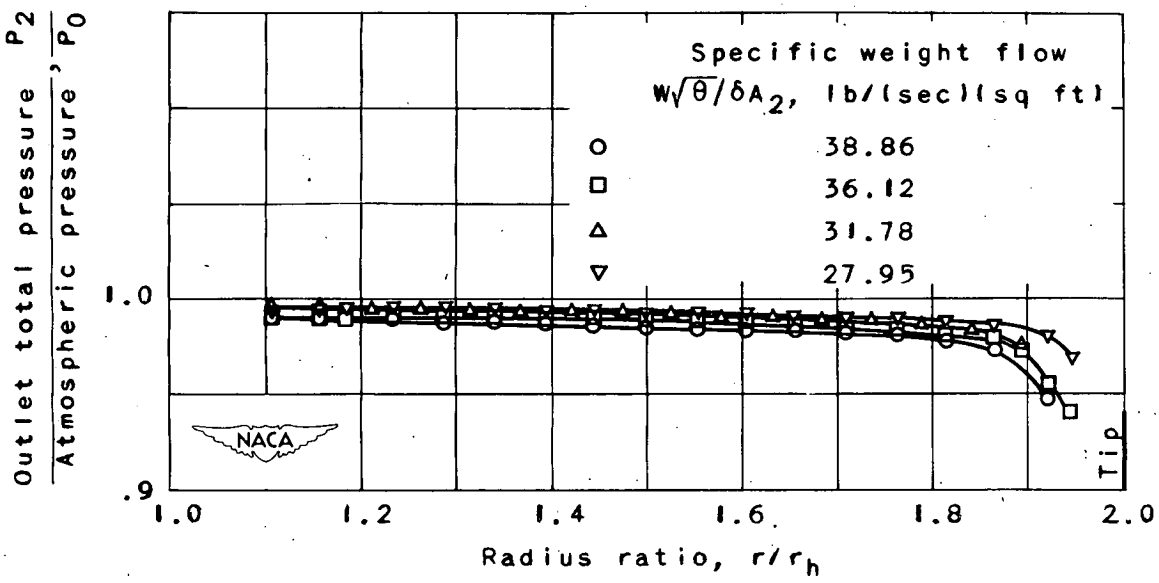

Figure 6. - Radial distribution of ratio of outlet total pressure to atmospheric pressure.

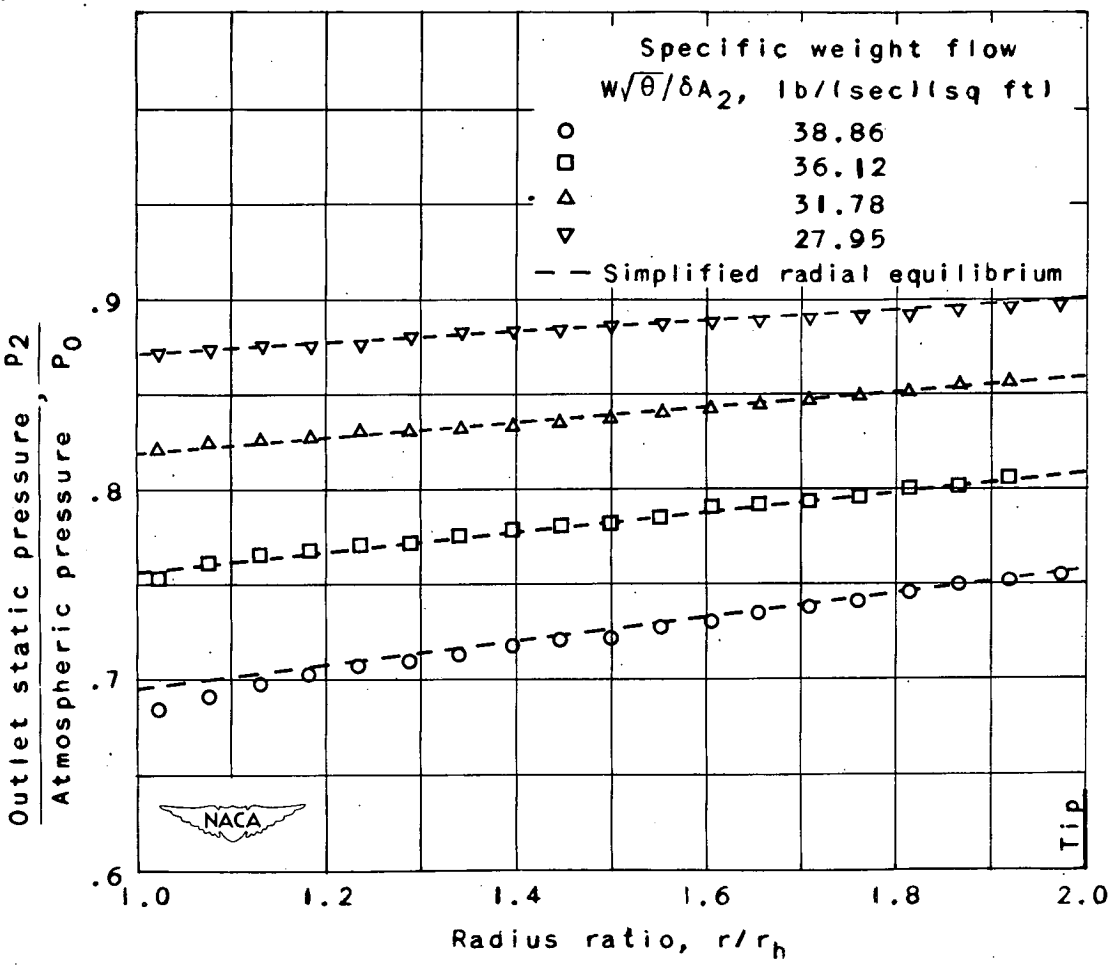

Figure 7. - Radial distribution of ratio of outlet static pressure to atmospheric pressure.

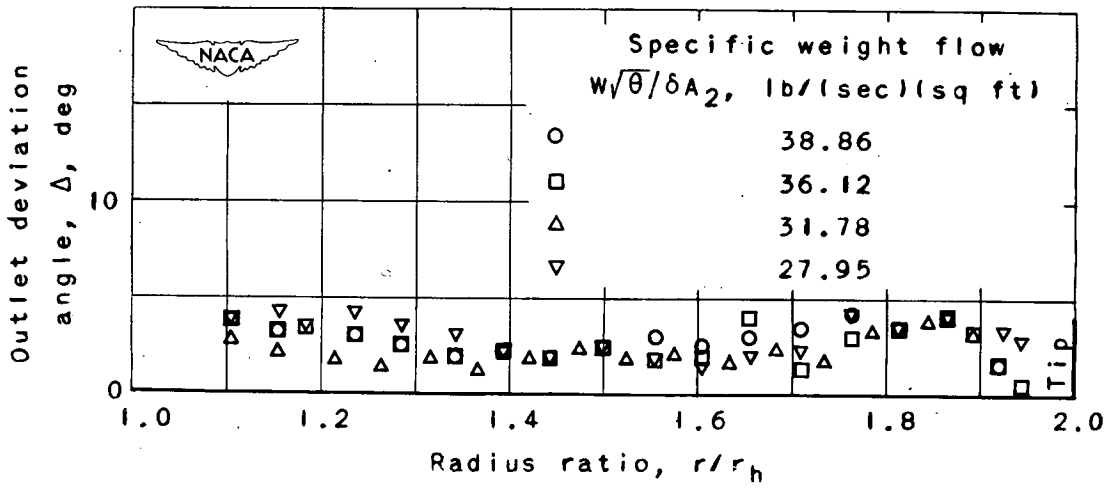

Figure 8. - Radial distribution of outlet deviation angle.

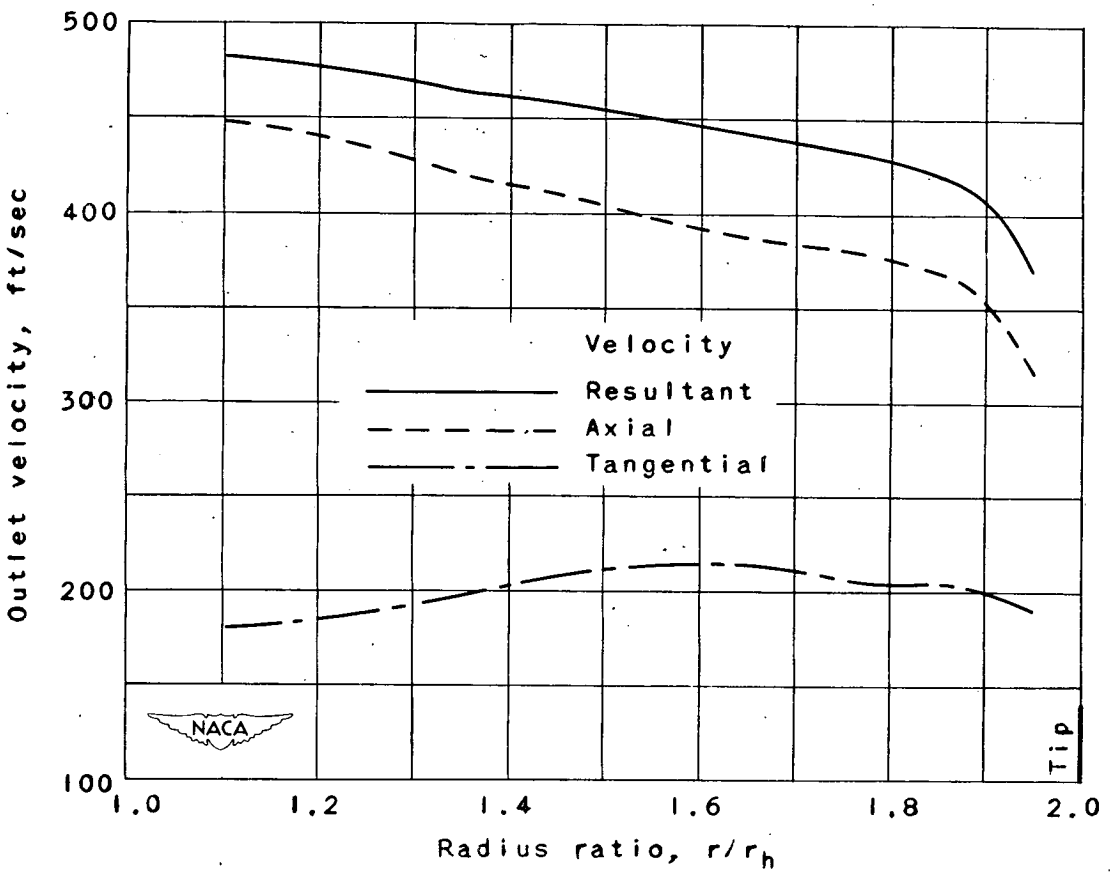

(a) Specific weight flow $W\sqrt{\theta}/\delta A_2$, 27.95 pounds per second per square foot.

Figure 9. - Radial distribution of outlet velocity.

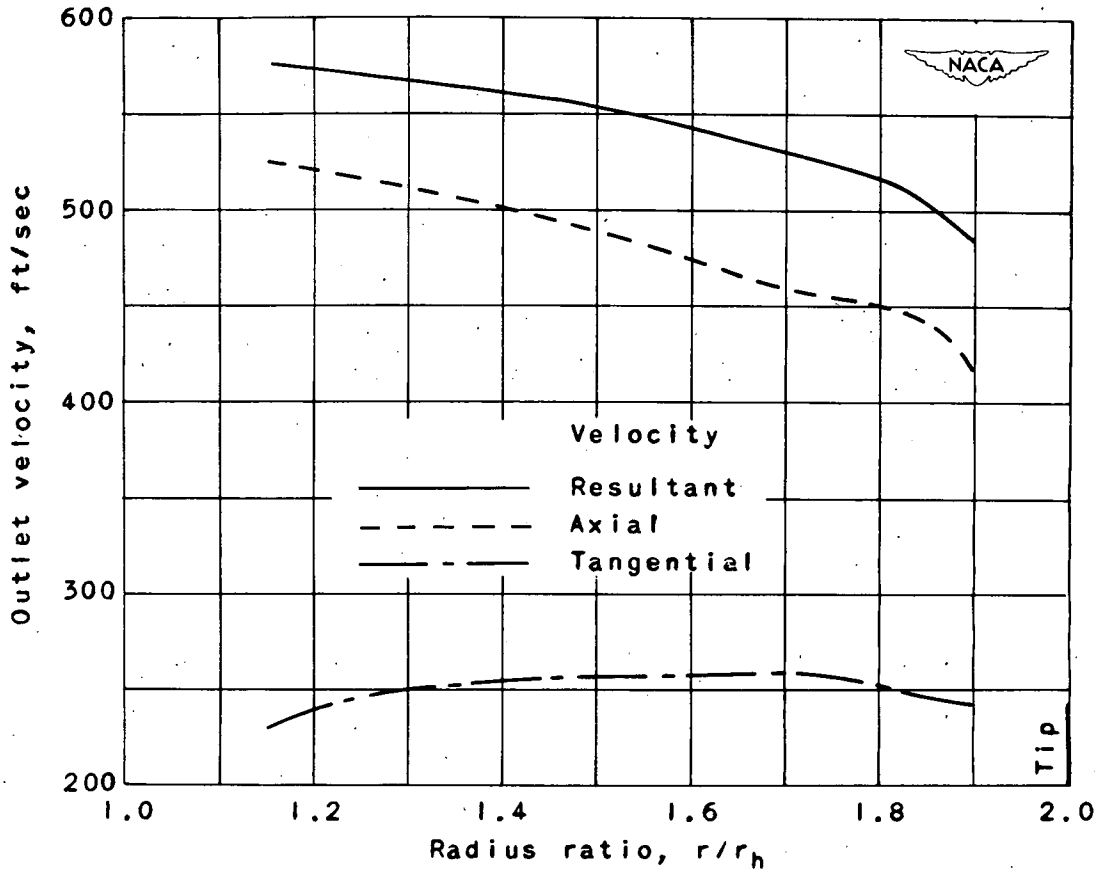

(b) Specific weight flow $W\sqrt{\theta}/\delta A_2$, 31.78 pounds per second per square foot.

Figure 9. - Continued. Radial distribution of outlet velocity.

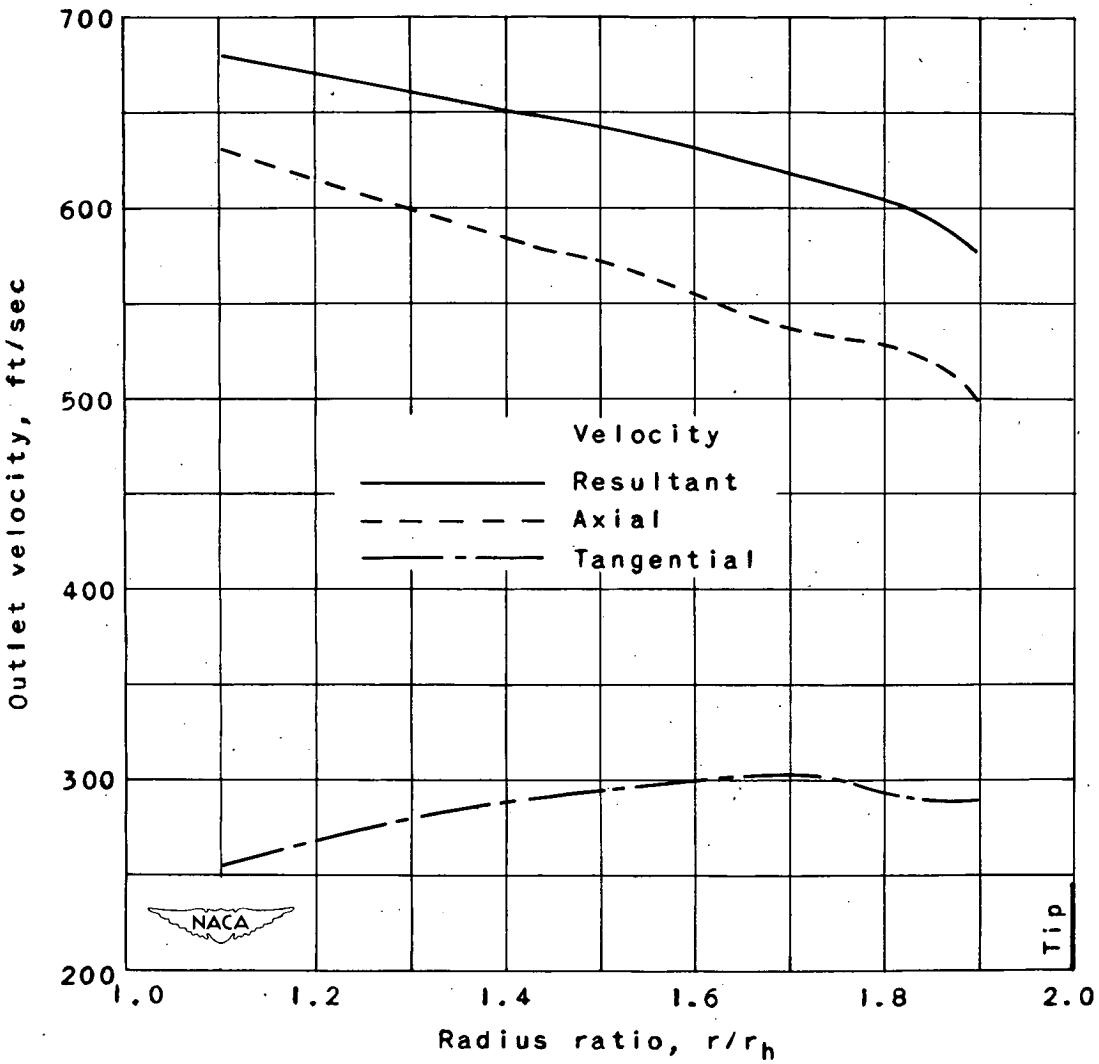

(c) Specific weight flow $W\sqrt{\theta}/\delta A_2$, 36.12 pounds per second per square foot.

Figure 9. - Continued. Radial distribution of outlet velocity.

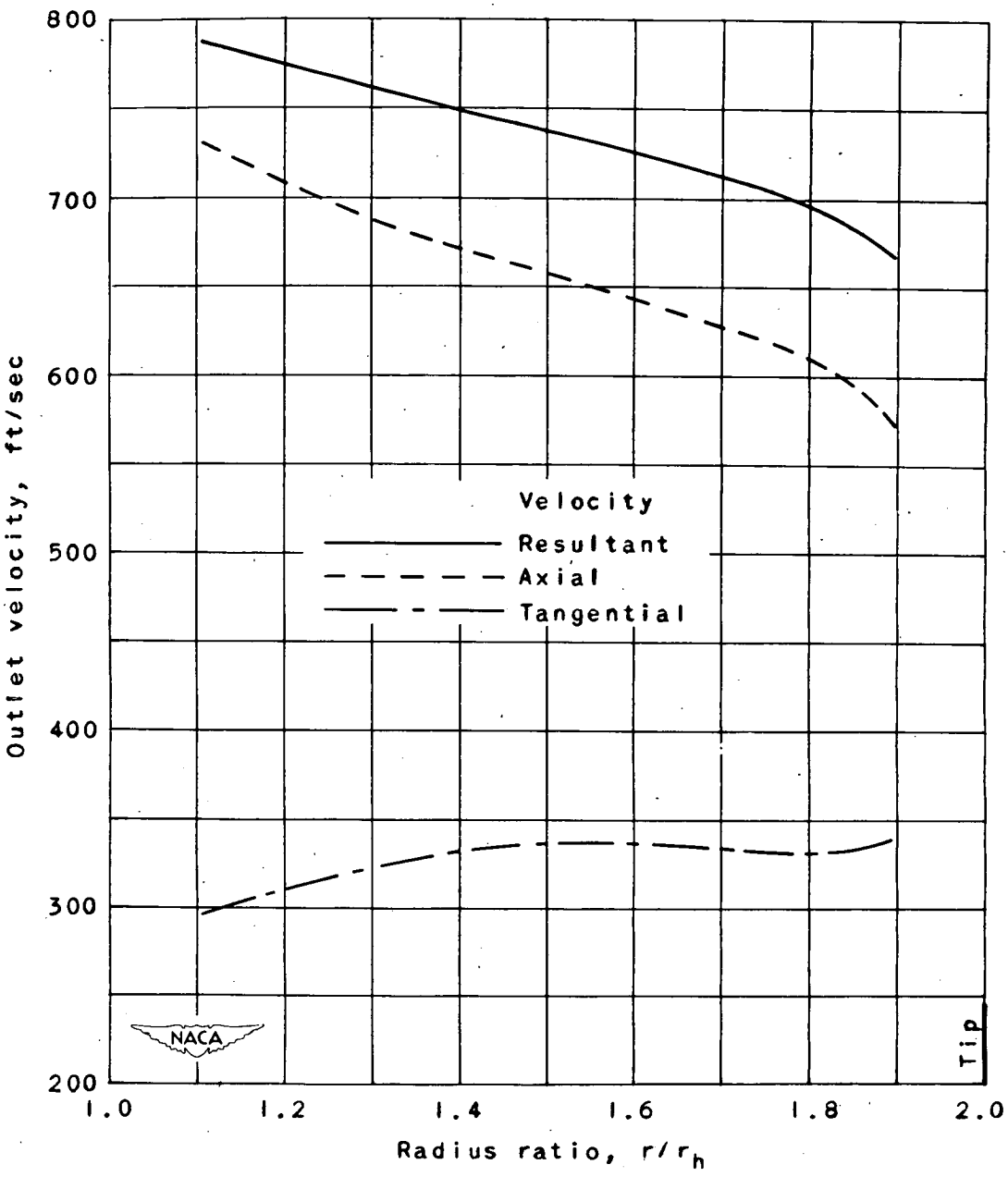

(d) Specific weight flow $W\sqrt{\theta}/\delta A_2$, 38.86 pounds per second per square foot.

Figure 9. - Concluded. Radial distribution of outlet velocity.

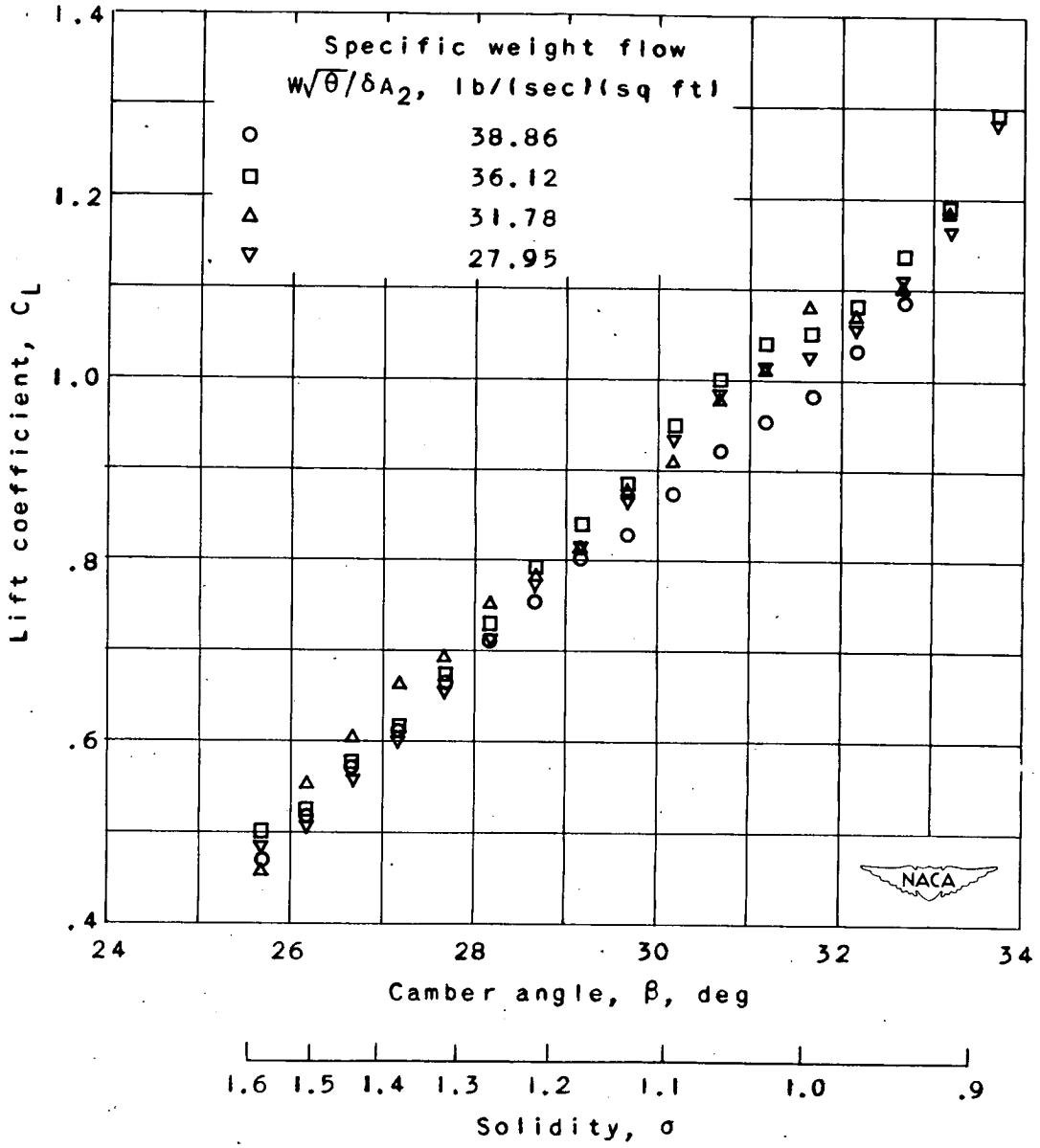

Figure 10. - Variation of lift coefficient with camber angle and solidity.

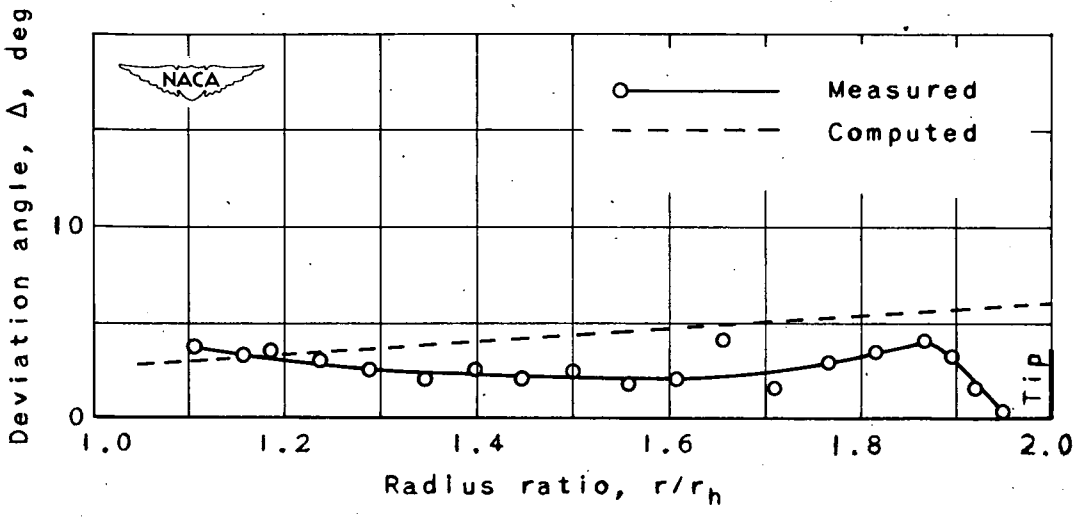

Figure 11. - Comparison of measured deviation angles with angles computed by rule based on Constant's work (reference 2) for specific weight flow of 36.12 pounds per second per square foot.

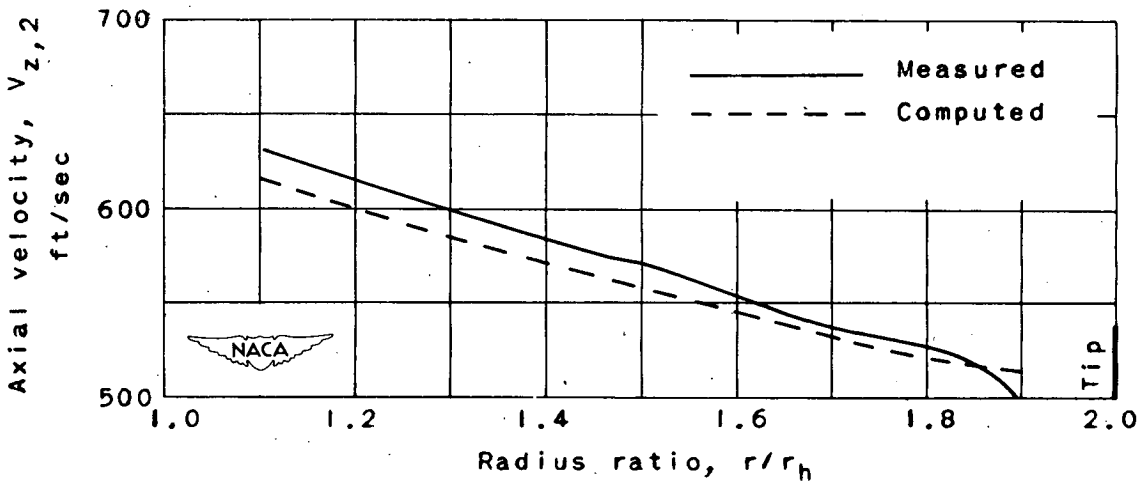

Figure 12. - Comparison of measured and computed axial velocities of outlet measuring station at specific weight flow of 36.12 pounds per second per square foot.

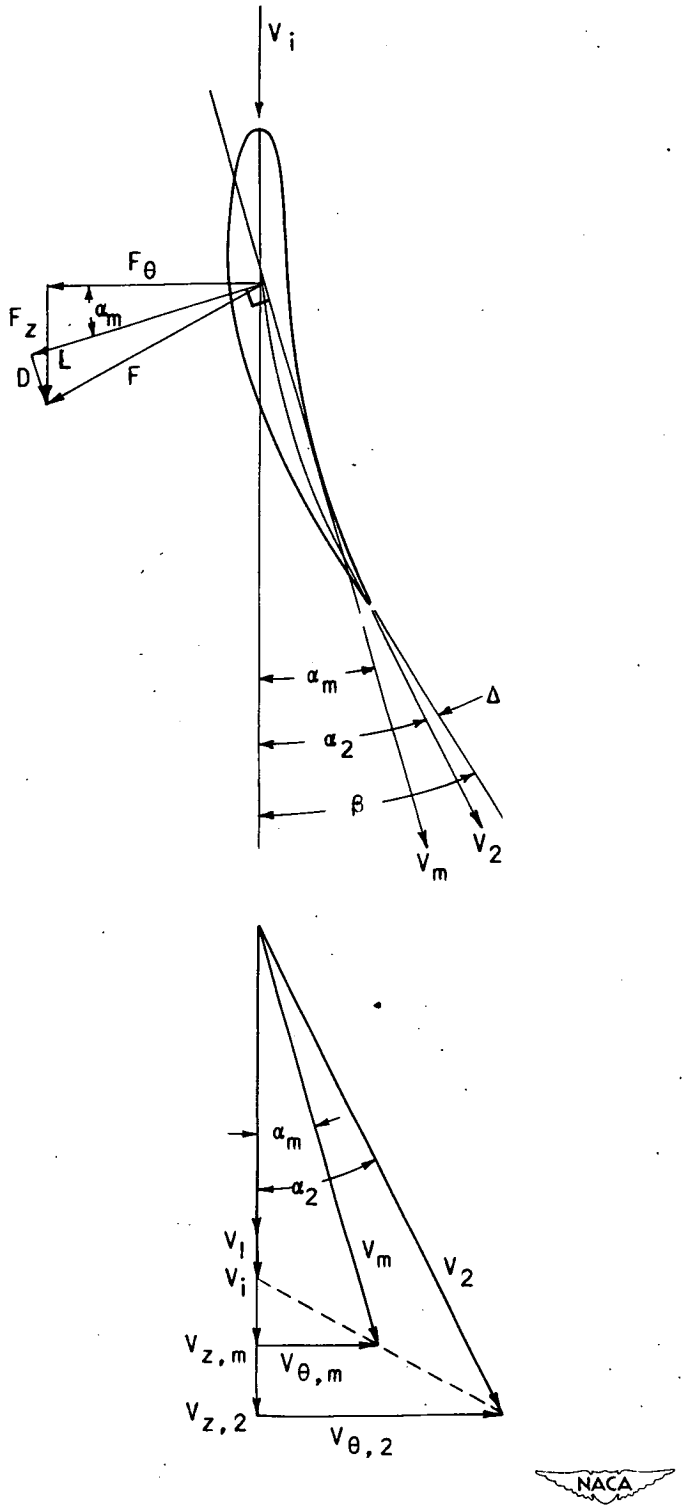

Figure 13. – Vector diagrams of forces on blade element and velocities through guide vanes.